Temperature Insensitive Fiber Optic Interferometer
and
Applications

by

Kent A. Murphy

Thesis submitted to the Faculty of the
Virginia Polytechnic Institute and State University
in partial fulfillment of the requirements for the degree of
Masters of Science
in
Electrical Engineering

APPROVED:

Richard O. Claus

Ahmad Safaai-Jazi

Ronald J. Pieper

October, 1989
Blacksburg, Virginia

Temperature Insensitive Fiber Optic Interferometer

and

Applications

by

Kent A. Murphy

Richard O. Claus, Chairman

Electrical Engineering

(ABSTRACT)

A method of modifying a fiber optic fused biconical tapered coupler to produce a relatively temperature insensitive Michelson interferometer is presented. The modification was accomplished by cleaving the coupler after the minimum taper region and polishing, perpendicular to the endface, to a point just short of the interaction region. This allows one of the two fiber cores, which are within micrometers of each other with their claddings fused together, to be coated at its endface with a reflecting material. This reflecting core serves as the reference arm, while the other core serves as the sensing arm. Variations in the method of fabrication of the sensor are described. Because of the close proximity and short length of the reference and sensing arms, the interferometer is temperature insensitive.

The miniaturized Michelson interferometer is characterized and its limitations are discussed. A surface acoustic wave detection scheme is successfully demonstrated. Results of a magnetic field sensor using the miniaturized Michelson interferometer and a magnetostrictive material are presented.

Acknowledgments

I would like to thank Dr. Richard O. Claus, my advisor, for giving me the opportunity to attend graduate school and to work at FEORC. I would also like to thank Dr. Ahmad Safaai-Jazi and Dr. Ronald J. Pieper for there useful discussions and for serving on my committee.

I am grateful to for helping every step of the way, from the beginning, when it was just an idea to the final written paragraph, with guidance, suggestions and hard work. I also wish to thank , and for their valuable suggestions and assistance during the experimentation, data gathering and the presentation of this work. A special thanks to and and the other members of FEORC for making this experience a pleasure.

Finally, I am deeply grateful for the love and support extended to me by my family especially my parents, and . Above all, I wish to thank my wife, , for her love and understanding during the long hours and for giving me the courage to try to be the best that I can be.

This research was sponsored in part by the Virginia Center for Innovative Technology and NASA Langley with contract monitor .

Table of Contents

List of Illustrations

1.0 Introduction

The Michelson interferometer, invented by Albert Michelson in 1880, is one of the most useful measuring devices in optics [1]. With the invention of coherent light sources (lasers) and the development of low loss, single-mode optical fibers, it has become relatively easy to build rugged interferometers such as the Michelson or the Mach-Zehnder. Single-mode fiber optic interferometric sensors (FOIS) have been shown to be among the most sensitive measurement devices available today [2]. In the mid 1970's, FOIS were suggested first for measurement of rotation and later for measurement of pressure, temperature and magnetic fields [3,4,5]. Fiber optic sensors are characterized as intrinsic or extrinsic. An intrinsic sensor uses the optical fiber itself as the sensing element. An extrinsic sensor uses the optical fiber only as a guide to transmit the light from the source to the sensing region and from the sensing region to the detector.

This thesis describes an extrinsic fiber optic sensor. The extreme sensitivity to temperature associated with all FOIS is a problem when the desired parameter to be measured is not temperature. This sensitivity to temperature is always present when the sensing and reference arms of the interferometer are physically at different locations. Minuscule changes in temperature difference between the sensing and reference arms affect the phase difference detected at the output of the sensor. This differential drift in the phases of the two arms caused by random fluctuations in temperature results in fading in the amplitude of the detected signal.

The objective of this thesis is to build a temperature insensitive Michelson interferometer. Thermal stability has been achieved by reducing the length and separation between the sensing and reference arms of a single-mode fiber optic coupler.

Chapter 2 briefly describes the theoretical aspects of the Michelson interferometer, single-

mode fiber optic couplers and the physics behind the temperature insensitive miniature FOIS. Chapter 3 includes details concerning the fabrication and characterization of the miniature FOIS.

Presented in Chapter 4 are applications of the miniature FOIS which include the detection of surface acoustic waves and magnetic fields. Conclusions are discussed in Chapter 5.

2.0 Theory and Physics of the Miniaturized FOIS

2.1 Michelson Interferometer

A basic type of interferometer is the Michelson. Other types of interferometers, such as the Mach-Zehnder or Fiseau, can be described as modified versions of the Michelson interferometer. A schematic of a Michelson interferometer, using a bulk optic beamsplitter, is shown in Figure 1a.

In an ideal case, the beamsplitter reflects 50% and transmits 50% of the incident wave. The reflected wave is reflected back to the beamsplitter by mirror 1 after traveling a distance 2X. The transmitted wave is reflected back to the beamsplitter by mirror 2 after traveling a distance 2Y. The waves are then recombined at the beamsplitter where half of the recombined wave goes to the detector and the other half goes towards the source and is of no interest here. The difference in optical path length between the two waves is [1]

$$\delta = 2 (Y - X) . \tag{1}$$

Optical detectors are not capable of detecting the phase of light; the detector only produces a current or voltage proportional to the time averaged power of the incident light. The intensity of the two superimposed waves, at the detector, can be described by

$$I = A^2 \cos 2\left(\frac{2\pi}{\lambda} \frac{\delta}{2} \right), \tag{2}$$

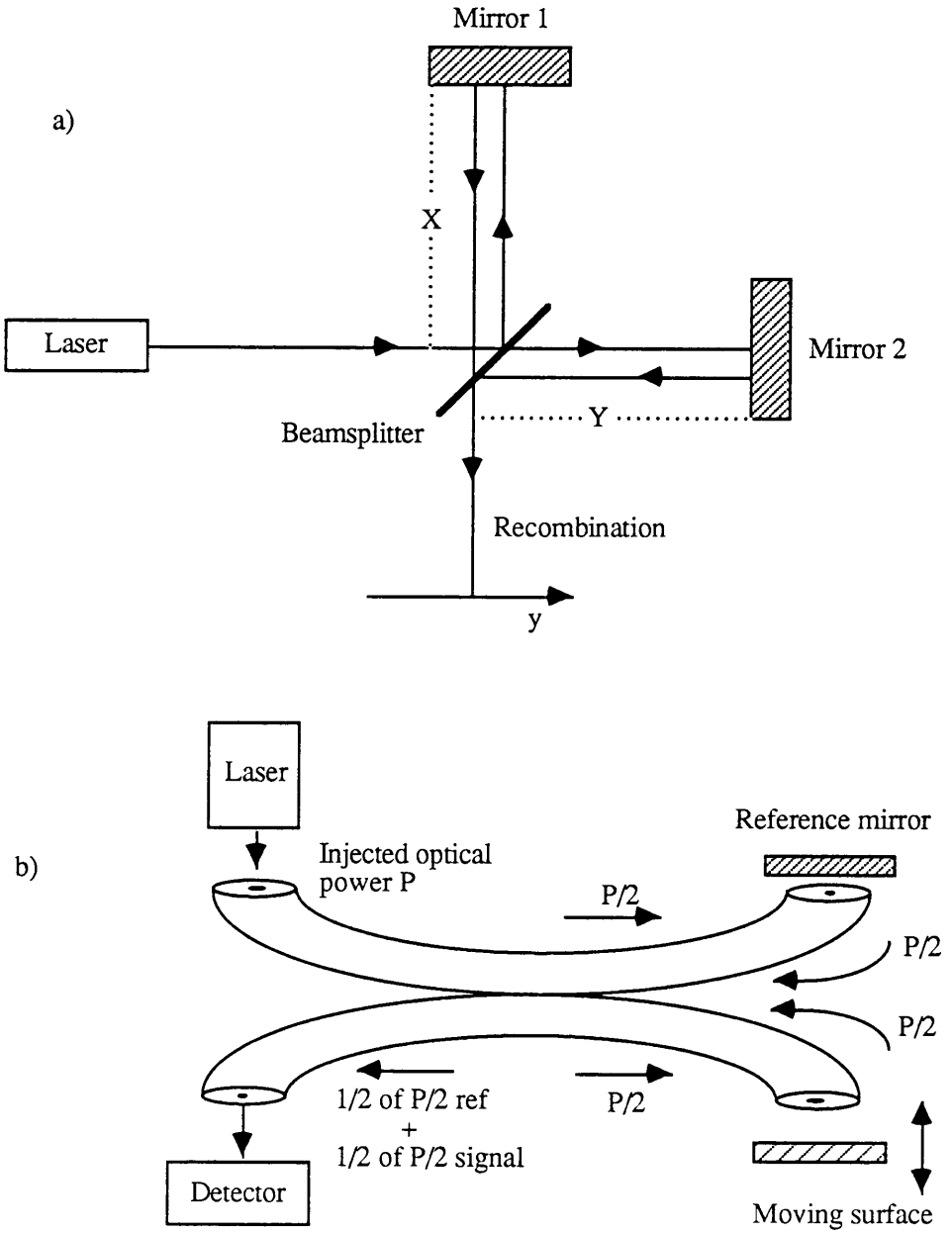

Figure 1. Michelson interferometers. a) Michelson interferometer, using a beamsplitter, with arms of unequal length X and Y. b) Michelson interferometer using a fiber optic coupler with an equal splitting ratio.

where I is the intensity, A is the maximum amplitude and λ is the wavelength of the light.

For

$$\delta = m\,\lambda\,, \tag{3}$$

there is constructive interference and for

$$\delta = \left(m + \frac{1}{2}\right)\lambda\,, \tag{4}$$

there is destructive interference, where m = 0, 1, 2, 3... .

2.2 Single-mode Fiber Optic Couplers

Single-mode fiber optic couplers have proven to be useful components in sensing as well as communication systems. In interferometric sensing schemes couplers are used to replace bulk optic beamsplitters. Schematics of two Michelson interferometers one using bulk optics and the other using a fiber optic coupler can be seen in Figures 1a and 1b. Couplers have several advantages including ease of implementation, smaller size and increased ruggedness.

Single-mode fibers can be manufactured by choosing the core radius and the indices of refraction of the core and cladding appropriately for a given wavelength as seen in Equation 5 [6].

$$V = \frac{2\pi a}{\lambda} \left(n_1^2 - n_2^2\right)^{1/2}, \tag{5}$$

where n_1 and n_2 are the indexes of refraction of the core and the cladding respectively and "a" is the radius of the core. For $V < 2.4$ only a single-mode is allowed to propagate [6].

The coupling coefficient between two identical single-mode fibers with a common cladding region is known to be [7]

$$C = \frac{\sqrt{2\Delta}\, U^2\, K_o\left(W\frac{d}{a}\right)}{a\, V^3\, K_1^2\,(W)}, \tag{6}$$

where

$$\Delta = \frac{n_1^2 - n_2^2}{2n_1^2}, \tag{7}$$

$$U = a\,k\left[n_1^2 - \left(\beta/k\right)^2\right]^{1/2},$$

$$W = a\,k\left[\left(\beta/k\right)^2 - n_2^2\right]^{1/2}.$$

Here K_o and K_1 are modified Bessel functions of the second kind, V is the normalized frequency described in equation 5, and k is the free-space wavenumber (2π/wavelength). As seen in equation 6, the coupling between two single-mode optical fibers is strongly dependent upon d, the distance between the two fiber cores, or the fiber diameter.

There are three basic fabrication methods used to produce single-mode fiber optic couplers [2]. All three methods control the spacing between the cores of the two fibers. Figures 2 a,b, and c show basic diagrams for the three methods of fabrication. Figure 2a is an etched coupler, the two fibers are twisted and the cladding is etched, using hydrofluoric acid, until the desired coupling is achieved. Figure 2b is a polished coupler , the two fibers are curved with a large radius and then the cladding is polished to within

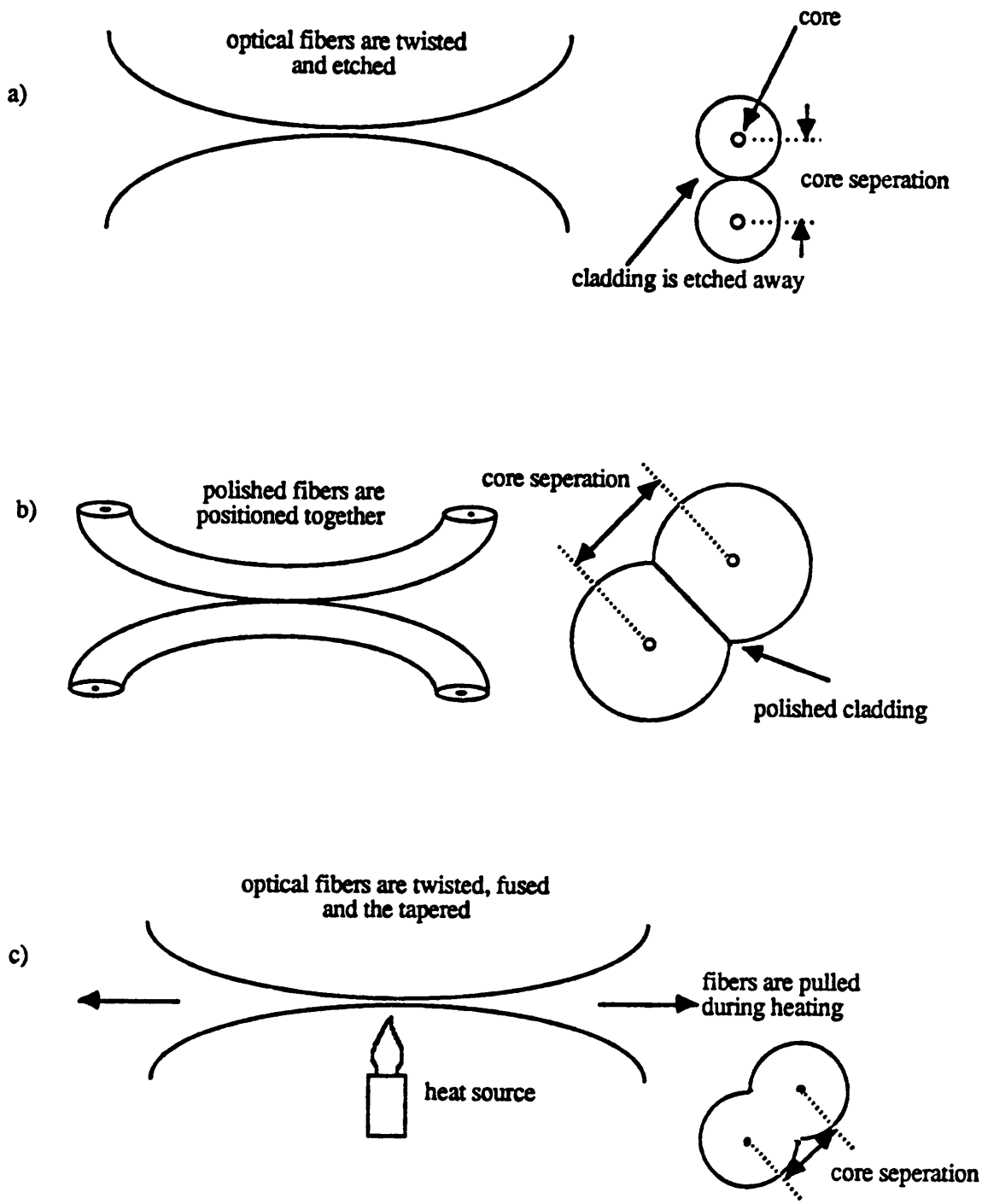

Figure 2. Single mode fiber optic couplers. a) Etched coupler. b) Polished coupler. c) Fused biconical taper coupler.

microns of the core. The two fibers are then positioned to obtain the desired coupling. The third method, and the method used here, is the fused biconical taper, seen in Figure 2c. The two fibers are twisted and then fused together and tapered with a heat source. This tapering allows the two cores of the fiber to become closer together. The fibers are tapered until the desired coupling has been accomplished.

One can assume a parabolic taper shape defined by [8]

$$a(z) = a_f\left(1 + \gamma z^2\right), \tag{7}$$

where z is the axial coordinate of the fiber with the origin at the center of the taper, a_f is the fiber radius at $z = 0$ and γ is a constant for the taper.

Combining Equation 5 and Equation 7, Burns and Abebe have used [8]

$$\frac{a_f^{7/2}}{L\left(\frac{a_f}{a_o}\right)^{1/2}} = 0.008\ \mu m^{5/2}. \tag{8}$$

as the defining equation for a tapered coupler with equal outputs, where L is the total taper length and ao is the initial fiber radius before tapering.

2.3 Thermal Compensation Schemes in Fiber Optic Interferometric Sensing Systems

Single-mode couplers are typically used to replace bulk optic beamsplitters in interferometric configurations. As discussed earlier in the introduction, a major problem associated with fiber optic interferometric systems is signal fading due to thermal drifts. Several methods have been devised to eliminate these thermal drifts.

One such method consists of using a piezoelectric cylinder with the reference arm of the interferometer coiled around it [9]. The piezoelectric cylinder is driven by an error signal, generated from the interferometer output, in an effort to keep the interferometer in quadrature and prevent signal fading. The piezoelectric cylinder method is not useful in systems for the detection of low frequency signals, similar in frequncy to the thermal drifts, and is considered bulky to implement in practical situations.

Other methods to compensate for thermal drifts in Mach-Zehnder interferometer sensors include a two wavelength interferometer, two polarization interferometers and an interferometer using a 3x3 directional coupler [10]. All three of these methods produce two outputs that are always $\pi/2$ out of phase. The two outputs can be used in several different ways to stabilize the quadrature point of the sensor but all of the methods reduce the sensitivity of the sensor.

Also reported is a method using a common path for the sensing and reference arms in a heterodyne scheme [11]. The common path results from using the Fresnel reflection from the fiber/air interface interfered with the reflection from the surface to be monitored. This heterodyne system is extremely sensitive with a dynamic range of 86 dB , but is

limited to low frequency detection.

2.4 Technical Approach of the Miniaturized FOIS

The approach presented in this work is somewhat different from the work previously reported. Instead of trying to compensate for thermal drifts, the approach here is to reduce the thermal drifts. The method consists of reducing the length of the sensing and reference arms of a Michelson interferometer constructed of a modified single mode fiber optic coupler.

The modification results in a coupler with the two arms shortened to a point in the coupler where the light is coupled. Although this modification makes it difficult to quantify its temperature independence, in Section 3.2 experimental procedures are described which have been used in an attempt to characterize the miniaturized FOIS' dependence on temperature.

3.0 Experimental Techniques

3.1 Fabrication of the Modified Michelson Interferometer

A station for the fabrication of fused biconical taper fiber optic couplers was built. The 2x2 single-mode couplers were fabricated using a technique described by Slonecker [12]. Two optical fibers (4/125 μm single-mode at a wavelength of 633 nanometers), each approximately two meters in length, were placed on the coupler fabrication station. About four centimeters of coating was removed from the middle of the two meter long fibers.

The fibers were fused together and tapered using an oxygen and propane torch. One fiber was injected with a helium-neon laser at 633 nanometers, while both outputs were monitored using optical power meters. The fibers were tapered until approximately equal outputs on the two fibers were achieved. Excess losses of less than 0.75 dB were considered acceptable.

When the desired coupling had been achieved, the coupler was mounted on a four centimeter strip of Invar® and encapsulated in epoxy. The epoxy covered the coupler from the coating on the injected side to just a few millimeters past the minimum taper region on the detection side as seen in Figure 3. After the epoxy had cured, the part of the coupler that was not encapsulated in the epoxy was cleaved with a diamond scribe, broken off and discarded. The Invar® strip was mounted in a polishing fixture with phenyl salicylate as seen in Figure 4. The coupler was first ground to the proper length,

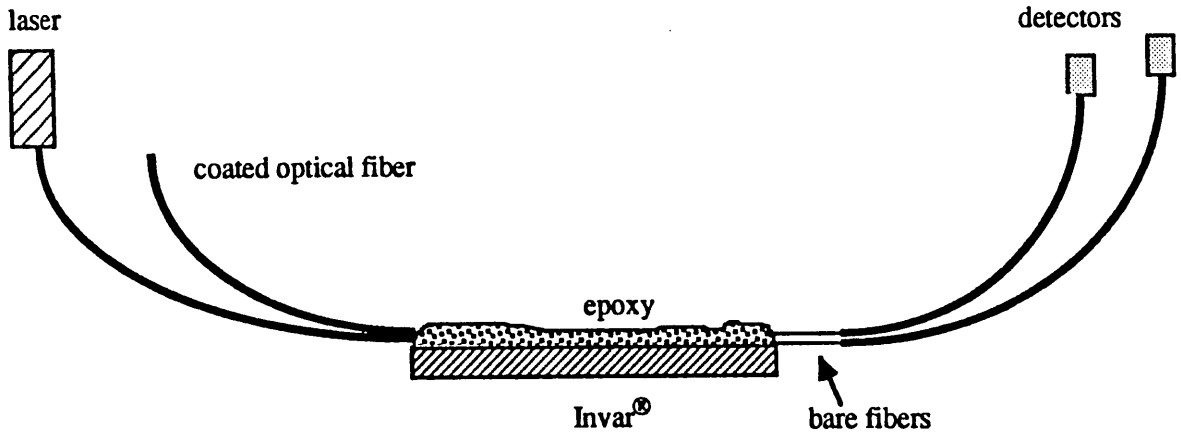

Figure 3. Encapsulting the coupler.

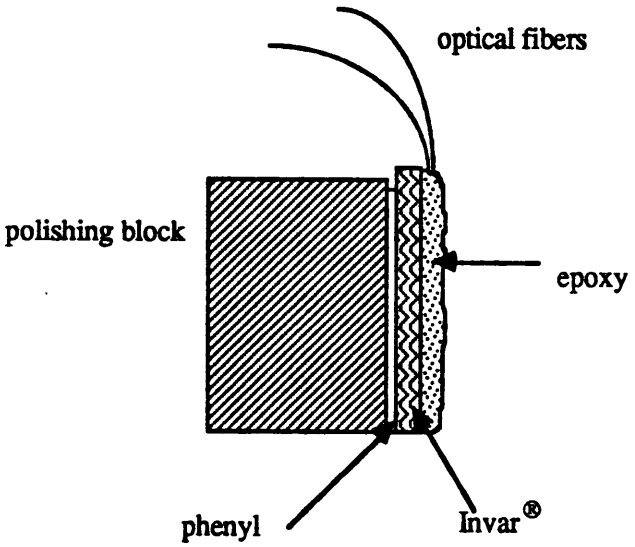

Figure 4. Coupler mounted for polishing.

just short of the coupling region, with 240 grit paper on a wet grinding wheel. Next the large pits were removed using 600 grit paper. The coupler cross-section was then visible upon inspection under a microscope. A final polish was done using a one micron polishing pad. A drawing of the resulting endface can be seen in Figure 5.

One of the cores of the coupler must be mirrored to serve as the reference arm. Four different methods were used to obtain a mirrored surface. The first attempt used a chemical silver deposition mixture to mirror one core. The core to be used as the sensing arm was covered with photo-resist under a microscope. After the silver was deposited on the coupler, the photo-resist was removed exposing the core for the sensing arm, while the reference core retained the silver coating. The chemical silver deposition method resulted in a poor reflection on the reflected core and an unclean surface on the other core. The modified Michelson was tested and was observed to be thermally stable, but had a low signal-to-noise ratio (SNR). These poor results were probably due to a lack of experience with the chemical deposition process and not an indication of the method itself.

The second method used the photo-resist to cover one core while the coupler was coated with aluminum in a vacuum deposition chamber. The coated fibers were protected with aluminum foil. The results were again poor because of an unclean reflecting surface on the reference core.

In the third attempt, aluminum foil was used to cover one of the cores during the aluminum deposition. The aluminum foil was placed over one of the cores under a microscope and then secured underneath the fixture used to hold the coupler during the deposition process. Figure 6 shows the coupler with the mirror coating. This method gave the best results for the modified Michelson interferometer even though the best reflection achieved was only 40%, which is much lower than the expected value of greater than 80% for aluminum.

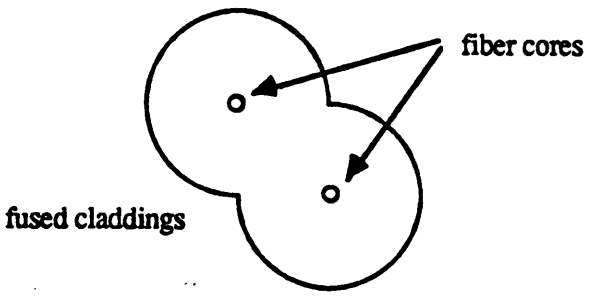

Figure 5. Endface of the polished coupler.

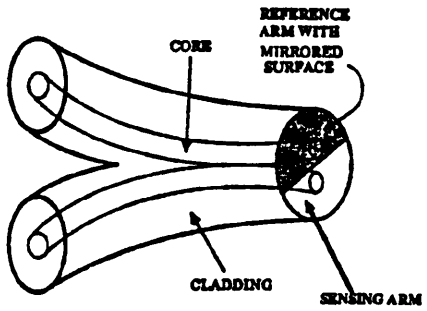

Figure 6. Detail of miniature Michelson interferometer.

The epoxy used to encapsulate the coupler for polishing damages the vacuum pump or the deposition chamber. Therefore a fourth method that does not require the coupler to be placed in the deposition chamber, was devised. The fourth method consisted of coating one half of a microscope cover slip with aluminum and then breaking it into small pieces that were later placed on the end of the coupler over one core only.

The fourth method was used for the magnetic field sensor described in Section 4.2. All other results presented here are from modified Michelson interferometer fabricated by the third method. Couplers made using all four methods of fabrication are miniature forms of the Michelson interferometer with the reference and sensing arms of very short lengths and only microns apart, resulting in a minuscule temperature gradient across the two arms.

3.2 Measurement of Fundamental Interferometer Parameters

Several experiments were conducted to characterize the sensor and to identify its limitations. The first experiment determined a minimum detectable displacement for the sensor. The sensor was mounted on a five axis positioner and pointed at a mirror that was mounted on an audio speaker as seen in Figure 7. The alignment of the sensor to the mirror was performed by actively monitoring the output of the sensor while a function generator was driving the speaker with a sinusoidally varying voltage. The sensor was positioned to achieve the maximum signal, which corresponds to the maximum amount of light recoupled into the sensor after it is reflected from the mirror. The displacement of the speaker was set to give a varying phase differential in the sensing arm of the interferometric sensor of approximately π. The quadrature point of the sensor was set to a stable position for maximum fringe contrast using a micro-positioner. This π difference in phase corresponds to a displacement of the mirror equal to a quarter wavelength, $\lambda/4$. The minimum detectable displacement for this sensor is 0.75 Angstroms and was calculated as follows:

$$\text{minimum detectable displacement} = \frac{\lambda/4}{\text{SNR}}, \tag{9}$$

where the wavelength is 632.8 nm and the SNR was 33 dB. Reflectivities of less than 40% for the reference arm and photodetectors with high noise figures restricted the SNR to 33 dB. Theoretically, shot noise limited detectors should allow SNRs in the 70-80 dB range. The second experiment was conducted to measure the thermal stability of the miniaturized FOIS. A standard homodyne Michelson interferometer was positioned next

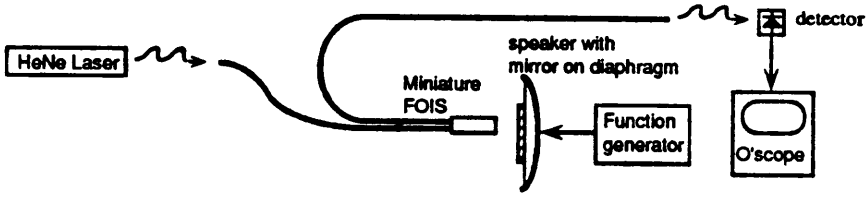

Figure 7. Experimental set-up for characterizing the miniature FOIS.

to the miniaturized FOIS in front of a mirror attached to a speaker as seen in Figure 8. The input conditions to the speaker were again set to give approximately a π phase shift for the two interferometers.

The sensing and reference arms of the homodyne Michelson interferometer were both approximately one meter in length. A phase shift differential of $\pi/2$ is expected between the two arms for a temperature gradient of only 10 millidegrees for a homodyne Michelson interferometer with sensing and reference arms of one meter in length each [2]. The homodyne Michelson interferometer did not employ compensation for drifts in signal due to temperature fluctuations.

The outputs of the two sensors were monitored continuously to observe any phase drifts due to small temperature changes in the environment. These drifts in phase can be seen as a fading of the output signal. Figures 9a - c show the output signals of the two interferometric sensors at arbitrary times. The homodyne Michelson interferometer suffered continuous drifting of the detected signal. Figure 9a shows the comparison when the homodyne Michelson interferometer had drifted to a maximum signal. The fading signal of the homodyne Michelson interferometer compared to the stable signal of the miniaturized Michelson interferometer, can be seen in Figures 9b and 9c.

The excitation of the speaker then was set to give larger displacements of the mirror which results in multiple fringes in the outputs of the two interferometers. Signal fading was again observed in the homodyne Michelson interferometer while the miniaturized Michelson interferometer remained stable. Oscilloscope traces of this comparison are presented in Figures 10a and 10b.

Two additional experiments were conducted in an effort to explore some of the limitations of the miniaturized Michelson sensor. The first experiment was performed to evaluate the loss of signal versus the separation of the sensor from the vibrating surface.

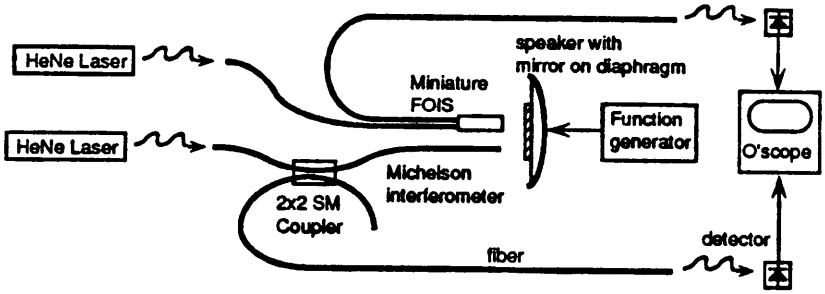

Figure 8. Experimental set-up for comparing miniature FOIS and homodyne Michelson interferometer.

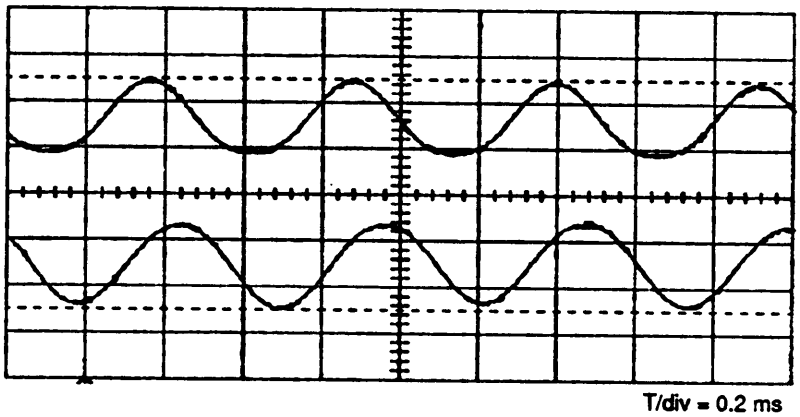

Figure 9(a). Comparison of miniature FOIS (the top trace) and classic Michelson interferometer (the bottom trace) at time T=0.

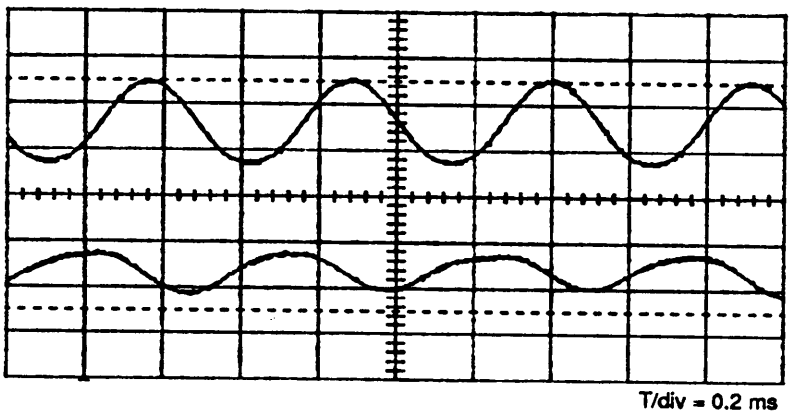

Figure 9(b). Comparison of miniature FOIS (the top trace) and classic Michelson interferometer (the bottom trace) at time T=100ms.

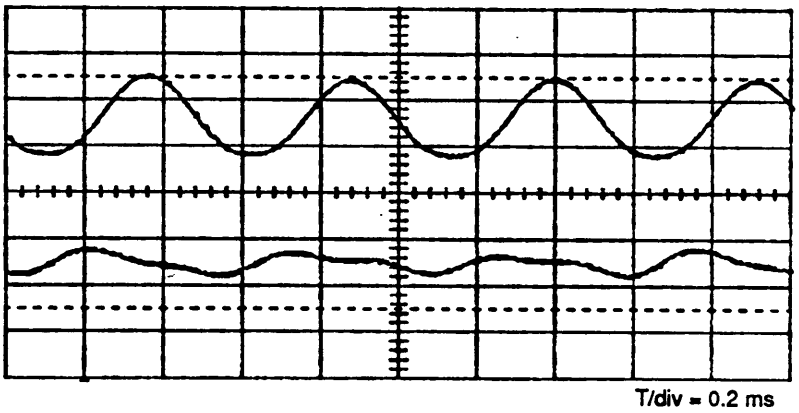

Figure 9(c). Comparison of miniature FOIS and classic Michelson interferometer at time T= 200 ms.

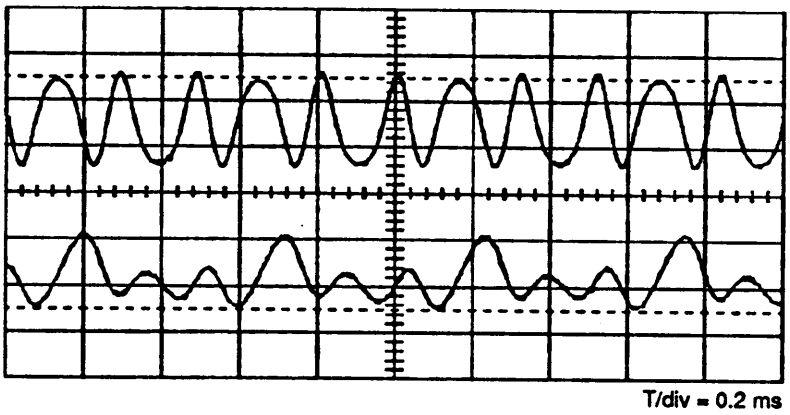

Figure 10(a). Comparison of miniature FOIS and classic Michelson interferometer at time T=0 with multiple fringes.

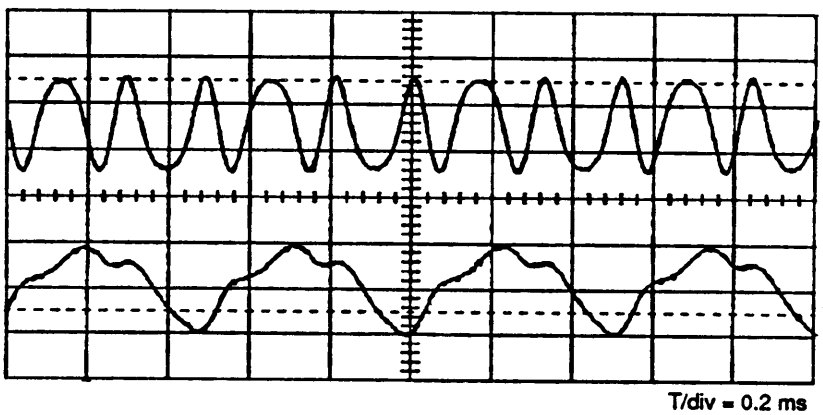

Figure 10(b). Comparison of miniature FOIS and classic Michelson interferometer at time T = 100 ms for multiple fringes.

The experimental set-up is shown in Figure 11. The modified Michelson sensor was positioned in front of a vibrating mirror mounted on an audio speaker, as described earlier in Section 3.2. The input conditions to the speaker were set to give a varying phase differential of approximately π in the two arms of the interferometer. The sensor was positioned as close to the vibrating mirror as possible without touching the surface of the mirror. At the closest point an output voltage, ΔV, was recorded as a reference. The positioner was used to move the sensor away from the mirror by a distance z, as seen in Figure 11.

At each discrete location, z, the fringe contrast was maximized by adjusting the micrometer on the positioner and that maximum ΔV was recorded. A normalized plot of ΔV versus z is presented in Figure 12. An expanded version of the ΔV versus z can be seen in Figure 13, where it is easy to see that for approximately 30 microns of z displacement from the vibrating surface the signal has dropped by 3 dB.

The second additional experiment was conducted to give an estimate of the sensor sensitivity to angular misalignment. The extreme sensitivity of the sensor to angular misalignment made it difficult to carry out the measurement. The experimental set-up was identical to the set-up for the measurement of sensitivity to longitudinal separation except that a long thin rod was attached to the sensor described in Figure 14. The small displacement at the tip of the rod was measured using digital calipers. The angle of the sensor was controlled by the micro-positioner. The output signal of the miniaturized FOIS was adjusted for maximum fringe contrast and that position was considered to be $\theta=0$. The measurements for angular misalignment were approximate (only four data points were taken), but it gives an idea of just how sensitive the sensor is to changes in the angle θ. The plot of the normalized data is presented in Figure 15. For an angle of only 0.06 degrees the output signal dropped by approximately 3 dB.

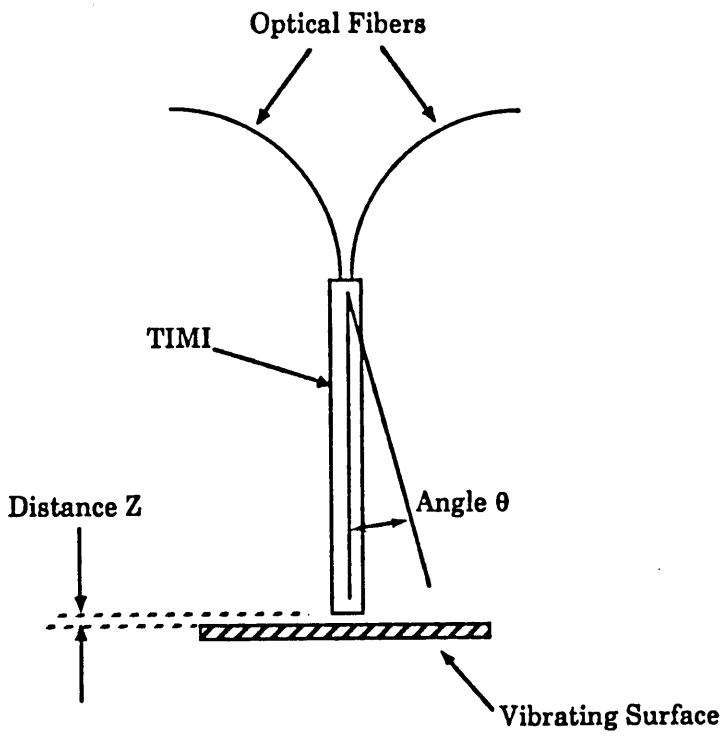

Figure 11. Experimental set-up for sensor sensitivity to distance z.

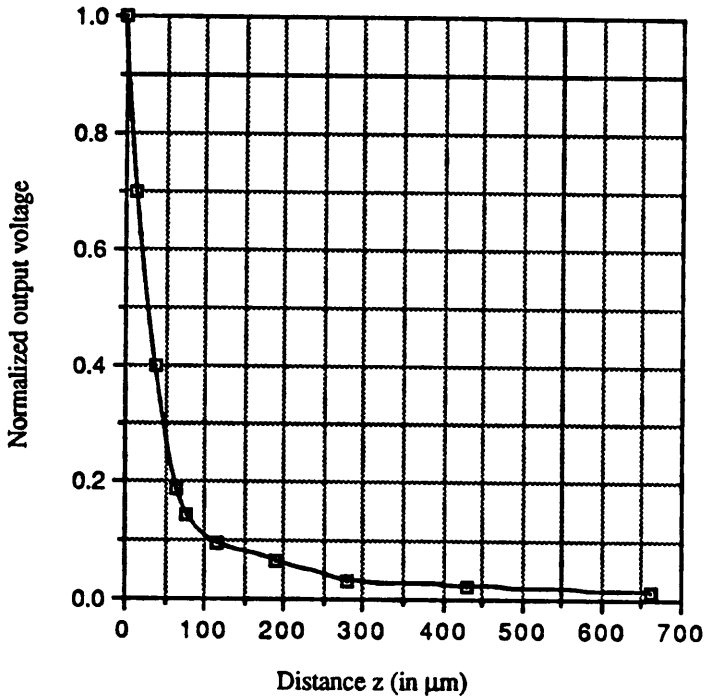

Figure 12. Normalized output versus the distance z from the surface.

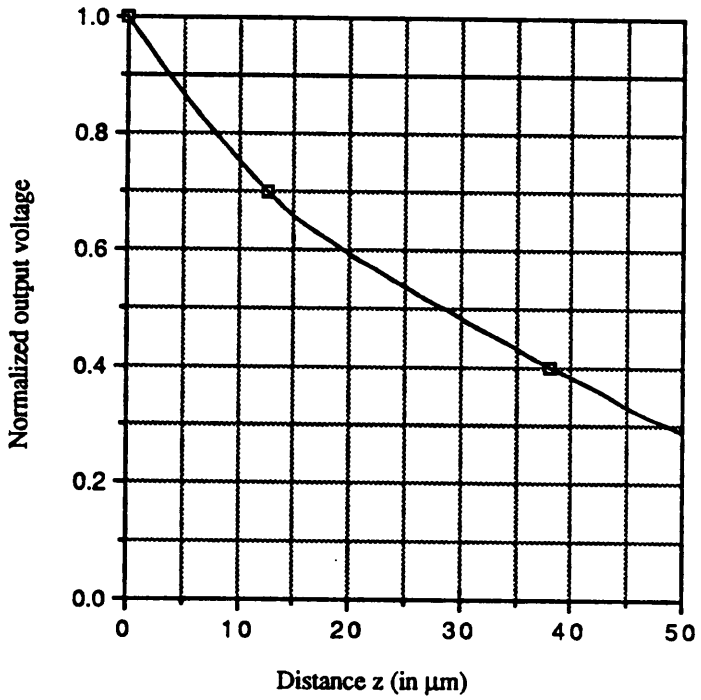

Figure 13. Normalized output versus the distance z from the surface.

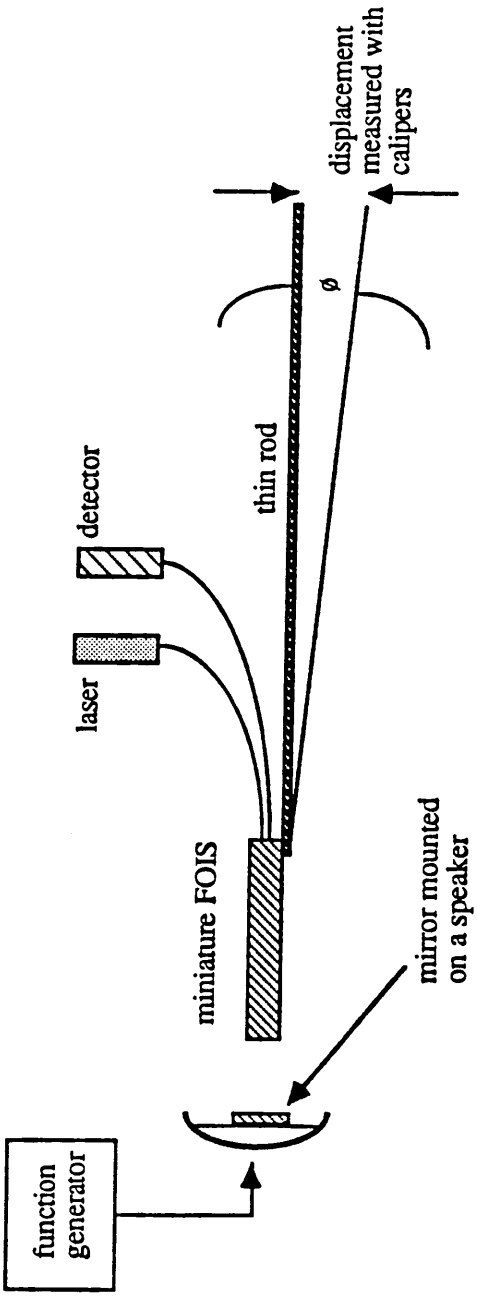

Figure 14. Angular misalignment set-up.

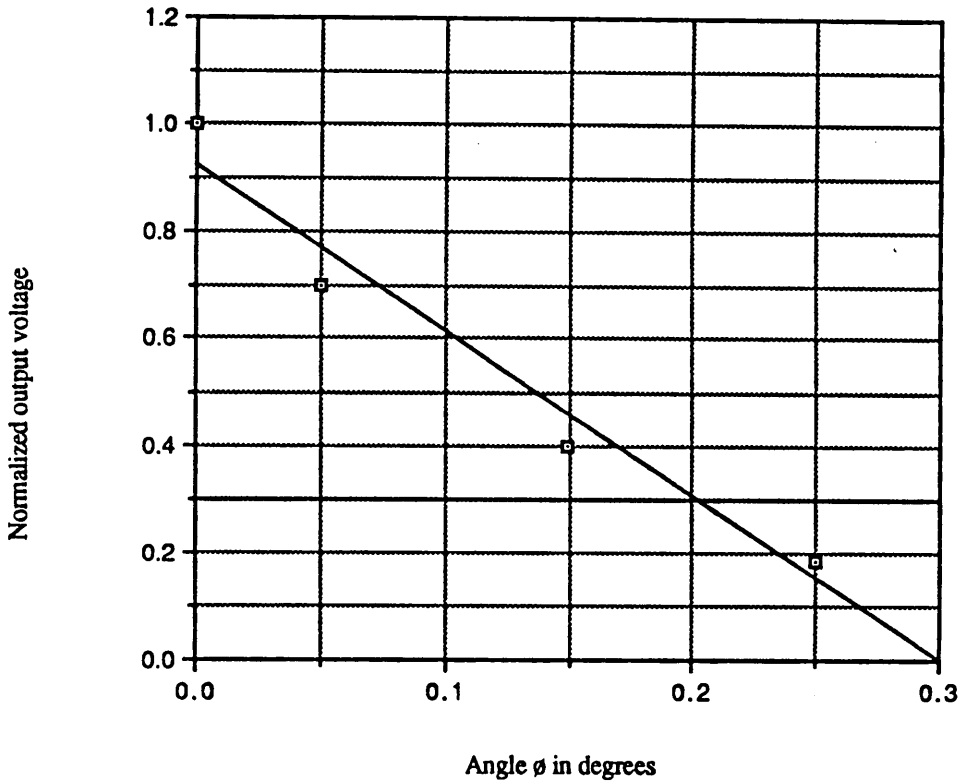

Figure 15. Angular sesitivity plot.

Another limitation of the sensor is the difficulty in adjusting the quadrature point (Q-point). The only way to adjust the Q-point is by changing the position of the entire sensor. This adjustment could be done by placing the sensor on a piezoelectric transducer. However, the Q-point drift is not a problem if the sensor is mounted on something stable relative to the object that is displaced.

4.0 Applications

4.1 Surface Acoustic Wave (SAW) Detection

The detection of ultrasonic surface acoustic waves has been shown to have important applications in the non-destructive inspection and evaluation of materials. The generation and detection of SAWs are conventionally done using piezoelectric transducers (PZT).

The particle (atomic or molecular) oscillation associated with SAW motion generally follows an elliptical orbit (at the surface) with the major axis of the ellipse perpendicular to the surface along which the waves are traveling [13]. The minor axis of the ellipse is parallel to the direction of wave propagation as seen in Figure 16. The energy is exponentially decaying into the material and is generally confined to within a few wavelengths of the surface. SAWs can exist in more complex forms than the one shown in Figure 16, but are variations of the simplified wave shown. SAW displacements are usually on the order of a few Angstroms. Researchers have reported many different methods for using optical methods for the detection of acoustic signal, [14 - 20].

The miniature FOIS has several advantages over PZTs for the detection of surface acoustic waves. 1) The miniature FOIS does not have to be in contact with the surface of the material. The contact with the surface the PZT requires can affect the SAW. 2) The miniature FOIS can operate at higher temperatures than conventional PZTs. 3) The material and geometry of PZTs determine certain resonant frequencies at which they are most sensitive. This resonant frequency limits the PZT bandwidth. The miniature FOIS is bandwidth limited only by the detector electronics which make the miniature FOIS useful from DC to the GHz range.

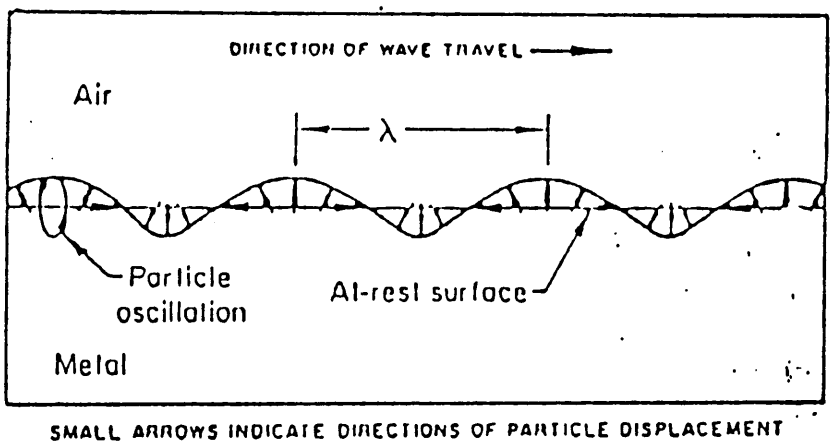

Figure 16. Diagram of surface waves where λ is the wavelength [12].

The experimental set-up for the SAW detection is presented in Figure 17. Surface acoustic waves were generated along an aluminum bar with a 1MHz Harisonic PZT, with an 80 degree angle of incidence.The PZT was powered by a MATEC radio-frequency gated amplifier at a frequency of 1 MHz. A 5X lens was used to focus 633 nm light from a 10mW helium-neon laser into the input optical fiber of the miniature FOIS. The optical detector was an avalanche photo diode (APD). The miniature FOIS was mounted on an adjustable tripod stand as seen in Figure 18. The tripod stand allows the miniature FOIS to be positioned for the maximum signal by adjusting the height and the angle of the sensor . The tripod also allows the miniature FOIS to be moved along the bar easily.

For the detection of SAWs, an envelope detection scheme was used and the signal was averaged 1000 times. An oscilloscope trace of the signal from the miniature FOIS and the received signal by the PZT can be seen in Figure 19. Figure 20 is an oscilloscope trace of the output of the miniature FOIS in real-time (not averaged) along with the PZT received signal. Vibration of the tripod, relative to the aluminum bar, is responsible for the high noise level and could possibly be reduced by devising a more sophisticated way of holding the miniature FOIS.

In Figure 21 the output signal of the miniature FOIS was stored in the oscilloscope and then the sensor was moved approximately 4 cm and the output signal stored again. The 13.6 micro-second delay in the detected signals leads to a SAW velocity of 2940 m/s, which is close to the SAW velocity for aluminum, 2790 m/s, obtained form standard handbooks [13]. A SAW velocity of 2940 m/s was also measured experimentally using a PZT detection method.

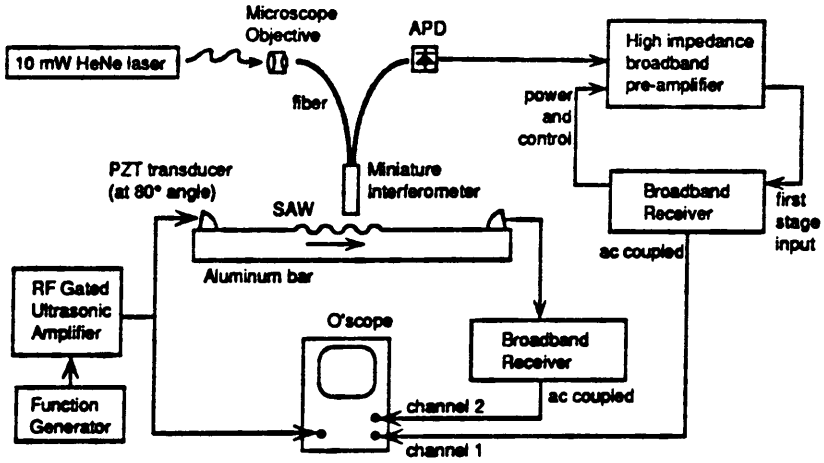

Figure 17. Experimental set-up for SAW detection

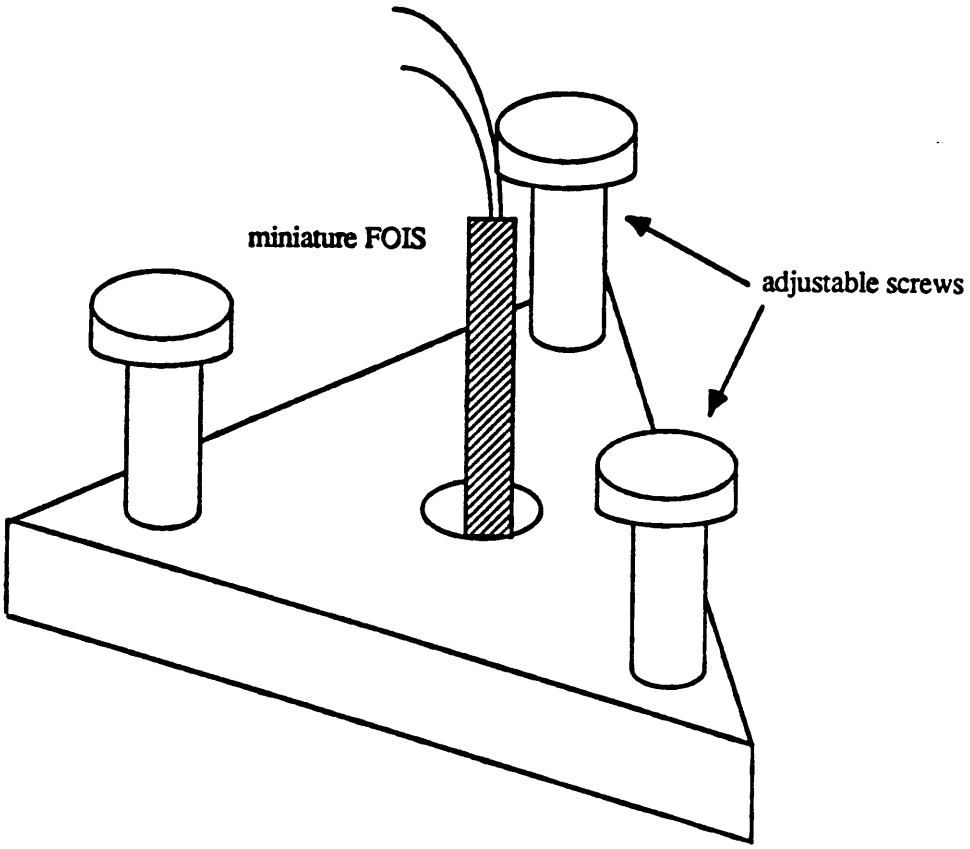

Figure 18. Tripod stand to adjust the height and angle of the sensor relative to a surface.

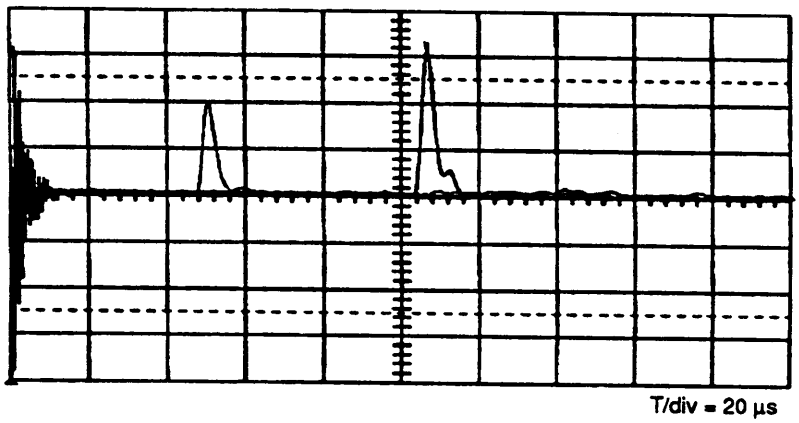

Figure 19. Oscilloscope output showing miniature FOIS response (left) and pulse detected by piezoelectric transducer (right).

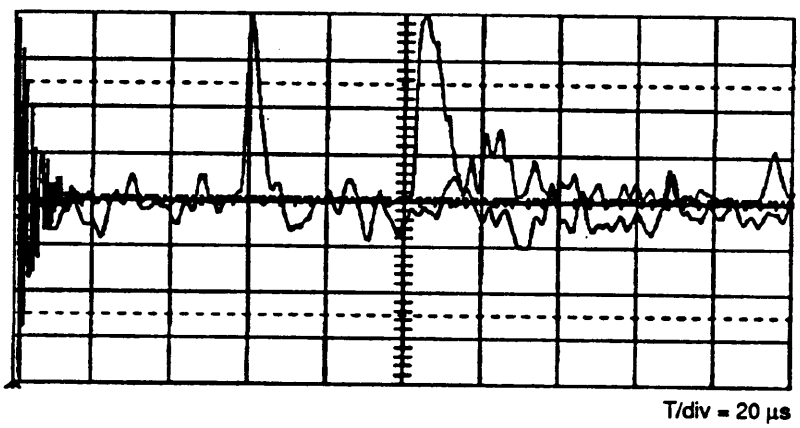

Figure 20. Real-time (not averaged) SAW detected by minature FOIS (left) and classic Michelson interferometer (right).

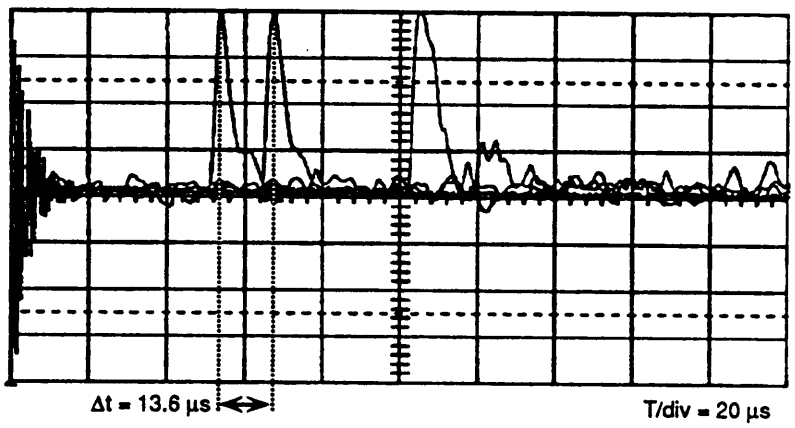

Figure 21. Oscilloscope output showing detection of SAW by minitaure FOIS at two locations separated by 4 cm.

4.2 Magnetic Field Sensing

Magnetostrictive materials are commonly used as strain transformers in fiber optic magnetic field sensors [5,21]. Metallic-glass alloys are commonly used due to their availability. One of the most widely reported metallic-glass magnetic field sensors is unannealed $Fe_{74}\ Co_{10}\ B_{16}$.

The magnetic field sensor reported here is built using a relatively new material called Terfenol®. Terfenol® is composed of $Tb_{0.3}Dy_{0.7}Fe_2$ and is reported by the manufacturer to have a high magnetostriction compared to other commercially available metallic glasses. A diagram of the magnetic field sensor is presented in Figure 22. A small mirror was attached to the end of the Terfenol to increase the reflection, which improves the sensitivity of the sensor. The Terfenol rod expands and contracts with temperature fluctuations. These fluctuations were detected by the miniature FOIS and are seen as noise. In an attempt to compensate for the fluctuations the miniature FOIS was mounted on a iron rod which has a similar coefficient of thermal expansion as the Terfenol®. Although this procedure did not completely compensate for the fluctuations, it did reduce them enough to acquire data.

A schematic of the experimental set-up can be seen in Figure 23. A Helmholtz coil is used to generate "ac" magnetic fields proportional to the input current [22]

$$H = \frac{N\,I}{L}, \tag{10}$$

where H is the magnetic field intensity in Oersteds, N is the number of turns of the coil, L is the length of the coil in meters and I is the current, in amps, in the coil.

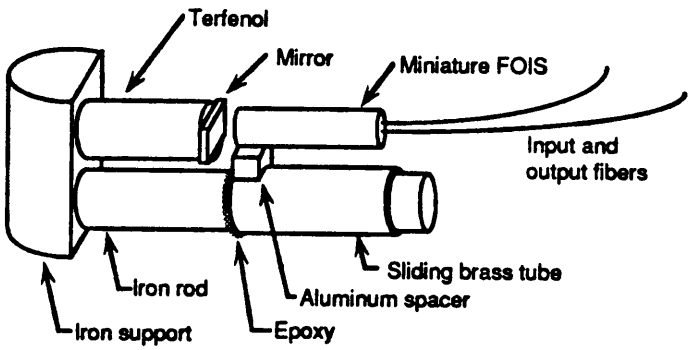

Figure 22. Detail of mounting scheme for miniature FOIS and magnetostrictive Terfenol[•].

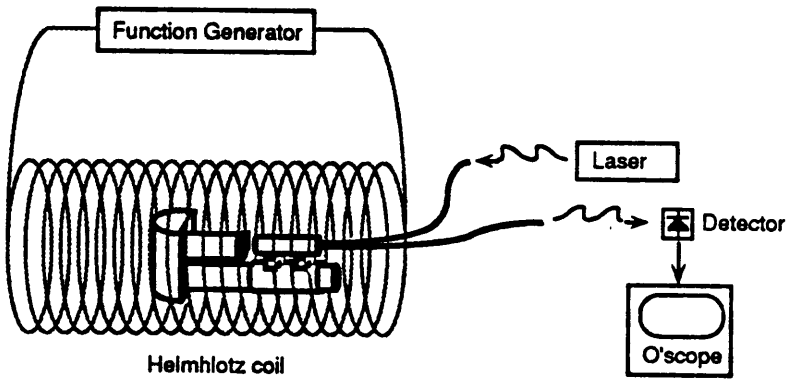

Figure 23. Experimental set-up for magnetic field sensing.

The input to the coil was such that it produced a 3.5 kHz magnetic field that oscillated from zero to a value limited by the output of the function generator. The output (ΔV) of the sensor was recorded at ten different settings of the input to the coil. A plot of the input in Oersteds versus ΔV out for the sensor can be seen in Figure 24.

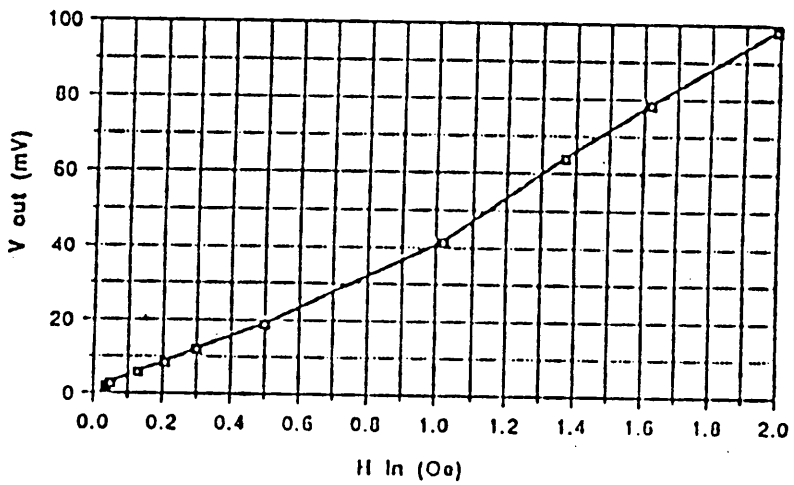

Figure 24. Output of miniature FOIS used as a magnetic field sensor.

5.0 Conclusions

A miniature FOIS has been developed and demonstrated to have no thermal drifts when compared to a homodyne Michelson interferometer. Measurement of displacements with sub-Angstrom resolution was demonstrated.

One of the basic limitations of this sensor design is that it can be used only for the measurement of external perturbations that manifest themselves as displacements. While adjusting the quadrature point of operation of the sensor is possible by mounting the entire sensor on a PZT, this could prove to be a limitation.

The sensor was demonstrated in a SAW detection scheme with advantages over conventional PZT detection methods. These advantages of the miniature FOIS over PZTs include higher operating temperatures, non-contact with the surface and higher bandwidth. The sensor was also used to construct a magnetic field detector using Terfenol®.

Future work could include constructing a temperature sensor by splicing a piece of single-mode fiber on to the unmirrored "sensor" core of the coupler. The sensitivity of the temperature sensor would be dependent upon the length of the spliced single-mode fiber. Another configuration to be considered would be using the modified coupler, with neither core mirrored, as a differential interferometer. The change in intensity observed at the output of the sensor would correspond to the difference in phase of the two reflected beams from a given surface.

References

1. Moller K.D., Optics, University Science Books, California, 1988.

2. Culshaw B., Optical Fibre Sensing and Signal Processing, Peter Peregrinus, London, 1984.

3. Bucaro J.A., Dardy H.D. and Carome E.F., "Optical Fiber Acoustic Sensor", Applied Optics, v16, p. 1761,1977.

4. Hocker G.B., "Fiber-optic Sensing of Pressure and Temperature", Applied Optics, v 18, p. 1445, 1979.

5. Trowbridge F.R. and Phillips R.L., "Metallic-glass Fiber-Optic Phase Modulators", Optic Letters, v. 6, p. 636, 1981.

6. Keiser G., Optical Fiber Communications, McGraw-Hill, New York, 1983.

7. A. W. Snyder and J. D. Love, Optical Waveguide Theory, p. 392-393, Chapman and Hall, New York, 1983.

8. Burns W.K. and Abebe M. , "Coupling Model for Fused Fiber Coupler with Parabolic Taper Shape", Applied Optics, v. 26, p. 4190, 1987.

9. Jackson D.A. , Priest R. , Dandridge A. and Tveten A.B. "Elimination of Drift in a Single-mode Optical Fiber Interferometer Using a Piezoelectrically Stretched Coiled Fiber", Applied Optics, v. 19, p. 2926, 1980.

10. Sheem S.K., Giallorenzi T.G. and Koo K., "Optical Techniques to Solve the Signal Fading Problem in Fiber Interferometers", Applied Optics, v. 21, p. 689, 1982.

11. Laming R.I., Wilmhurst T.H., Halliwell N.A. and Baker J.R., "A Practical All-fibre Laser Vibrometer", SEM Conference, p. 774, 1989.

12. Slonecker M., "Fused Biconical Tapered Single Mode Coupler Research at ITT", Fiber Optic Sensor Systems Conference, Fort Eustis, Florida, 1987.

13. Metals Handbook, Nondestructive Inspection and Quality Control, American Society for Metals, v. 11, p. 485, 1976.

14. Monchalin J.P., "Optical Detection of Ultrasound", IEEE Transactions on Ultrasonics, Ferroelectrics and Frequency Control, v. UFFC-33, p. 1567, 1986.

15. Whitman R.L. and Korpel A., "Probing of Acoustic Surface Perturbations by Coherent Light", Applied Optics, v. 8, 1969.

16. Kline R.A. and Green R.E. Jr., "A Comparison of Optically and Piezoelectrically Sensed Acoustic Emission Signals", Journal of the Acoustic Society of America, v. 64, p. 1633, Dec. 1978.

17. Stegeman G.I., "Optical Probing of Surface Waves and Surface Wave Devices", IEEE Transactions on Sonics and Ultrasonics, Jan. 1976.

18. Sontag H. and Tam A.C. , "Optical Detection of Nanosecond Acoustic Pulses", IEEE Transactions on Ultrasonics, Ferroelectrics and Frequency Control, v. UFFC-33, p. 500, Sept. 1986.

19. Palmer C.H. and Green R.E. Jr., "Optical Detection of Acoustic Emission Waves", v. 16, p. 2333, 1977.

20. Claus R.O. and Turner T.M., "Practical Optical Sensors of Ultrasonic Waves", ASNT Spring Conference, March 1982.

21. Bucholtz F., Koo K.P., Sigel G.H. Jr. and Dandridge A., "Optimization of the Fiber/Metallic Glass Bond in Fiber-Optic Magnetic Sensors", Journal of Lightwave Technology, v. LT-3, p. 814, 1985.

22. Hayt W. M. Jr., Engineering Electromagnetics, McGraw-Hill, New York, 1981.

The vita has been removed from the scanned document